AEROSPACE REPORT NO.
TR-2010(8550)-7

MicroTribological Performance of Au-MoS_2 and Ti-MoS_2 Coatings with Varying Contact Pressure

February 15, 2011

Pantcho Stoyanov[1], Richard R. Chromik[1], David Goldbaum[1],
Jeffrey R. Lince[2], and Xiaolig Zhang[3]

[1]McGill University
Montreal, Quebec, Canada
[2]Space Materials Laboratory
Physical Sciences Laboratories
[3]Teer Coating, Ltd.
Worcestershire WR9 9AS, UK

Prepared for:

Space and Missile Systems Center
Air Force Space Command
483 N. Aviation Blvd.
El Segundo, CA 90245-2808

Authorized by: Engineering and Technology Group

This report was submitted by The Aerospace Corporation, El Segundo, CA 90245-4691, under Contract No. FA8802-09-C-0001 with the Space and Missile Systems Center, 483 N. Aviation Blvd., El Segundo, CA 90245. It was reviewed and approved for The Aerospace Corporation by Gary F. Hawkins, Principal Director, Space Materials Laboratory; and Warren G. Goda, Principal Director, Research and Program Development Office. David E. Davis was the project officer for the Mission-Oriented Investigation and Experimentation (MOIE) program.

This report has been reviewed by the Public Affairs Office (PAS) and is releasable to the National Technical Information Service (NTIS). At NTIS, it will be available to the general public, including foreign nationals.

This technical report has been reviewed and is approved for publication. Publication of this report does not constitute Air Force approval of the report's findings or conclusions. It is published only for the exchange and stimulation of ideas.

Luis Rodriguez
for Mr. Davis
SMC/EN July 8, 2011

David E. Davis
SMC/EA

REPORT DOCUMENTATION PAGE

Form Approved
OMB No. 0704-0188

1. REPORT DATE (*DD-MM-YYYY*)	2. REPORT TYPE	3. DATES COVERED *(From - To)*
15-02-2011		

4. TITLE AND SUBTITLE

MicroTribological Performance of Au-MoS_2 and Ti-MoS_2 Coatings with Varying Contact Pressure

5a. CONTRACT NUMBER
FA8802-09-C-0001

5b. GRANT NUMBER

5c. PROGRAM ELEMENT NUMBER

6. AUTHOR(S)

Pantcho Stoyanov, Richard R. Chromik, David Goldbaum, Jeffrey R. Lince, and Xiaolig Zhang

5d. PROJECT NUMBER

5e. TASK NUMBER

5f. WORK UNIT NUMBER

7. PERFORMING ORGANIZATION NAME(S) AND ADDRESS(ES)

The Aerospace Corporation
Physical Sciences Laboratories
El Segundo, CA 90245-4691

8. PERFORMING ORGANIZATION REPORT NUMBER

TR-2010(8550)-7

9. SPONSORING / MONITORING AGENCY NAME(S) AND ADDRESS(ES)

Space and Missile Systems Center
Air Force Space Command
483 N. Aviation Blvd.
El Segundo, CA 90245

10. SPONSOR/MONITOR'S ACRONYM(S)
SMC

11. SPONSOR/MONITOR'S REPORT NUMBER(S)

12. DISTRIBUTION/AVAILABILITY STATEMENT

Approved for public release; distribution unlimited.

13. SUPPLEMENTARY NOTES

14. ABSTRACT

Solid lubricant coatings with co-sputtered metal and MoS_2 have shown favorable macrotribological properties at a wide range of contact stresses and humidity levels. These materials are also candidates for use in microcontacts and micro-electromechanical systems (MEMS), but their performance at this scale is poorly understood. For this study, microtribological properties of Au–MoS_2 and Ti– MoS_2 coatings, with varying metal additives of less than 15 at%, were examined using a nanoindentation instrument. Titanium and gold were chosen for this study as metal additives due to their different influence on the mechanical properties of the coating. The hardness and reduced modulus of the coatings increased with the addition of metal, when compared to pure MoS_2. Reciprocating microscratch tests were performed with two spherical diamond tips (50 and 10 μm radii) in dry air. A range of normal loads were used between 0.2 and 5.0 mN. Friction and wear measurements were analyzed with respect to the variation in the contact pressure and compared to literature studies performed at the macroscale. Correlations were found between the coating mechanical properties, tip-coating adhesion, interfacial shear strength, and the formation of transfer films and tribofilms.

15. SUBJECT TERMS

Solid lubrication, Molybdenum disulfide, MoS_2, Sputter-deposition, Mocro-electromechanical Sysstems (MEMS), Microtribology

16. SECURITY CLASSIFICATION OF:			17. LIMITATION OF ABSTRACT	18. NUMBER OF PAGES	19a. NAME OF RESPONSIBLE PERSON
					Jeffrey Lince
a. REPORT	b. ABSTRACT	c. THIS PAGE	Leave blank	13	19b. TELEPHONE NUMBER *(include area code)*
UNCLASSIFIED	UNCLASSIFIED	UNCLASSIFIED			(310)336-4464

Note

Document entitled "Microtribological Performance of Au–MoS2 and Ti–MoS2 Coatings with Varying Contact Pressure," by Pantcho Stoyanov, Richard R. Chromik, David Goldbaum, Jeffrey R. Lince, and Xiaoling Zhang originally printed in *Tribol Lett* (2010) 40:199–211.

Tribol Lett (2010) 40:199–211
DOI 10.1007/s11249-010-9657-6

ORIGINAL PAPER

Microtribological Performance of Au–MoS_2 and Ti–MoS_2 Coatings with Varying Contact Pressure

Pantcho Stoyanov · Richard R. Chromik · David Goldbaum · Jeffrey R. Lince · Xiaoling Zhang

Received: 28 March 2010 / Accepted: 5 July 2010 / Published online: 18 July 2010

Abstract Solid lubricant coatings with co-sputtered metal and MoS_2 have shown favorable macrotribological properties at a wide range of contact stresses and humidity levels. These materials are also candidates for use in microcontacts and micro-electromechanical systems (MEMS), but their performance at this scale is poorly understood. For this study, microtribological properties of Au–MoS_2 and Ti–MoS_2 coatings, with varying metal additives of less than 15 at%, were examined using a nanoindentation instrument. Titanium and gold were chosen for this study as metal additives due to their different influence on the mechanical properties of the coating. The hardness and reduced modulus of the coatings increased with the addition of metal, when compared to pure MoS_2. Reciprocating microscratch tests were performed with two spherical diamond tips (50 and 10 μm radii) in dry air. A range of normal loads were used between 0.2 and 5.0 mN. Friction and wear measurements were analyzed with respect to the variation in the contact pressure and compared to literature studies performed at the macroscale. Correlations were found between the coating mechanical properties, tip-coating adhesion, interfacial shear strength, and the formation of transfer films and tribofilms.

P. Stoyanov · R. R. Chromik (✉) · D. Goldbaum
Department of Mining and Materials Engineering, McGill University, Montreal, QC H3A 2B2, Canada
e-mail: richard.chromik@mcgill.ca

J. R. Lince
Tribology Section, Spacecraft Materials Laboratory, The Aerospace Corporation, El Segundo, CA 90245, USA

X. Zhang
Teer Coating, Ltd., West Stone House, Berry Hill Industrial Estate, Droitwich, Worcestershire WR9 9AS, UK

Keywords Solid lubrication friction · Solid lubrication mechanisms · Molybdenum disulfide · Microtribology

1 Introduction

For a little more than a decade, the testing of nano- and micro-scale sliding contacts has been an important research area that seeks to improve the tribological performance of nano/micro-devices and to have a better understanding of a material's behavior during single and multi-asperity contacts [1–17]. Due to their applications in hard drives, diamond-like carbon (DLC) coatings have been well studied for their tribological behavior at these small length scales [12–18]. More recently, interest in other materials for microtribological applications has arisen. The demonstration of atomic-layer deposition of chalcogenides [19, 20], such as WS_2, has provided the opportunity to include these materials, as solid lubricants, in micro-electromechanical system (MEMS). Additionally, there has been interest in using high-metal additions to MoS_2 [8, 10] for the possible use of these coatings in micromotors, switches or actuators.

Co-sputtered metal–MoS_2 solid lubricant coatings have shown favorable macrotribological properties at a wide range of contact stresses and humidity levels [21–31]. However, their microtribological performance is not nearly as well studied. Previous research has been performed using an atomic force microscope (AFM) [8] and a nanoindentation instrument [32, 33] to investigate the influence of the gold content on the microtribological properties of MoS_2. It has been shown that higher gold content (i.e. 84 at% Au) shows the most promise for microtribological systems due to the better performance (i.e. lower coefficient of friction and lower wear rate) in humid

environments and at higher contact pressure [32]. Other recent studies [34, 35] have focused on lateral force microscopy of nanoparticles of MoS_2.

The co-sputtering of titanium with molybdenum disulfide results in similar effects on the macrotribological properties as the Au dopant. The addition of titanium increases the hardness and the wear resistance of the coating and makes it less sensitive to humid environments during tribological testing, as shown by Renevier [24]. While varying the Ti content between 3 and 11 at%, Simmonds [25] illustrated that there was a significant increase in the endurance life with the lower Ti content. No reports in the literature were found on the microtribology of these coatings.

At present, it is well known that the low friction and high-endurance life of metal–MoS_2 coatings are accomplished by the early formation of a stable and uniform transfer film (i.e. MoS_2 is transferred to the counterface) and tribofilm (i.e. a thin crystalline MoS_2 layer is formed on the worn surface), which can be directly correlated to a low interfacial shear strength. However, it still remains unclear if and how these tribological mechanisms change when decreasing the contact size to the microscale. The goal of this study was to investigate the influence of gold and titanium content on the microtribological properties of the co-sputtered molybdenum disulfide coatings developed by Lince [23] and Teer [28], and to compare the results to previous literature at the macro-scale. The friction measurements were analyzed as a function of the contact pressure and were correlated to the interfacial shear strength, the wear volume, and Raman spectroscopy of the wear track.

2 Experimental Procedure

Three coatings were studied in this work: sputtered MoS_2, co-sputtered Ti–MoS_2 (3.8 at% Ti), and co-sputtered Au–MoS_2 (11.2 at% Au). The gold and titanium concentration was measured using an energy dispersive spectrometer (EDS) on a field emission gun scanning electron microscope (Hitachi 4700-S FEG-SEM, Japan). The Au-containing and pure MoS_2 samples were produced at the Space Materials Laboratory of The Aerospace Corporation (El Segundo, CA, USA) using a custom sputter deposition system [23]. Briefly, coatings were deposited onto polished Si (100) wafers in a load-locked deposition chamber with a base pressure of 1.33×10^{-7} Pa (1×10^{-9} Torr). Separate Au and MoS_2 radio frequency sputtering sources were used, which were operated in unbalanced mode to increase the ion flux on the substrate surface during deposition. Argon (99.999% nominal purity) was used as the sputtering gas, and the Ar pressure in the chamber during deposition was typically 4 Pa (3×10^{-3} Torr). The Au and MoS_2 sputtering power densities were 0.25 and 3.0 W/cm^2, respectively. The titanium content samples were produced by Teer Coatings, Ltd. (Worcestershire, UK) using a close field unbalanced magnetron sputtering ion plating (CFUBMSIP) system operated in DC mode [28]. The preliminary chamber pressure before deposition was $5–6 \times 10^{-6}$ Torr. The argon-sputtering pressure was approximately 3.0×10^{-3} Torr. The distance between the target and substrates was about 150 mm. Substrates were rotated in front of each of the targets in turn in a speed of 4.0 rpm. A pulsed DC power supply provided −350 V bias on the substrates during the 15 min pre-cleaning and −30 V during deposition. A thin adhesion layer of Ti was produced first and followed by the Ti–MoS_2 coatings. The substrate temperature during the deposition process was lower than 200 °C.

The films were characterized with various methods to determine their structure, coating thickness, and roughness. Phase identification, bonding, and degree of crystallinity were examined using a inVia-Raman microscope (Renishaw, Gloucestershire, UK) with a 514.5 nm Ar + laser and X-ray diffraction (Bruker D8 Discover, Germany) in a standard Θ–2Θ geometry and with a Co-Kα X-ray source. The roughness of the coatings was measured using an atomic force microscope (AFM) (Veeco Dimension 3100, Santa Barbara, CA, USA) operated in contact mode using up to 50 μm by 50 μm scan size. The thickness of the coatings was measured from cross-sectional images obtained at high magnification using the FEG-SEM described above.

The mechanical properties of the coatings were measured with a Ubi 3 nanoindentation instrument (Hysitron, Inc. Minneapolis, MN, USA) with a 1D transducer and a diamond Berkovich tip. The hardness and reduced modulus values presented in this article are averages taken from roughly ten indentations using indentation depths of up to 56, 43, and 180 nm for the pure MoS_2, Au–MoS_2, Ti–MoS_2 coating, respectively. The same nanoindentation instrument and transducer were used for surface pull-off force measurements with a spherical diamond tip (50 μm tip radius) and the instrument in displacement control feedback mode. The maximum displacement throughout the test was 60 nm with a hold time of 1 s. The pull-off force was measured from the retracting adhesion force on the unloading curve [36].

The shape of the two diamond tips (10 and 50 μm radii) that were used for microtribology were characterized with an AFM (Veeco Nanoman 3100, Santa Barbara, CA, USA) operated in closed loop scanning in tapping mode. Scans were used to characterize the radius, roughness, and the area function of the spherical tips. This characterization was performed because, at smaller length scales, diamond

indenters typically deviate from the ideal spherical shape due to the difficulty of machining them [37]. Therefore, it is crucial to obtain an accurate area function (which is the cross-sectional area of the tip as a function of depth) in order to do any calculations that include the area of the tip as a variable. Over the depth range used for our tribological studies, the RMS roughness of the two tips were between 40 and 60 nm for the 10 μm tip and 5 and 15 nm for the 50 μm tip.

Tip area functions for both tips were produced using the AFM images and a custom-built pixel-counting algorithm created in Matlab Version 7.5.0 (The Mathworks, Natick, MA, USA). This procedure was similar to the one described by Bushby and Jennett [37]. The diamond tips were stationed vertically in a tip holder, without the ability of lateral and vertical movement. The indenter tips were scanned in the X and Y direction with scan sizes ranging from 5 to 30 μm. The scans were exported from the AFM software and converted into ASCII text files containing a 256 × 256 matrix. Each number in the matrix represents the height value, with the middle number in the matrix being the top of the tip. The column and row number represent the number of pixels as a function of the distance in the X and Y direction, respectively. In other words, each pixel represents a small square with the lengths being the scan size divided by 256 (i.e. the size of the matrix). Thus, using this matrix, the cross-sectional area of the tip can be calculated at any given depth, where the depth is the value in the matrix. Figure 1a and b shows the AFM images of the tips and plots of the area functions obtained from our pixel-counting algorithm compared to the ideal area functions for the 50 μm tip and the 10 μm tip, respectively.

Microtribological testing with the spherical diamond tips was conducted using a Ubi 3 nanoindentation instrument with a 2D transducer. Sliding tests were performed under controlled ambient temperature and a relative humidity between 3.0 and 5.0%. The relative humidity was controlled by flowing compressed air, which passed through anhydrous $CaSO_4$ (desiccant) and into the instrument enclosure at a high-flow rate for a few minutes and then a constant low flow rate throughout the sliding experiments.

The sliding experiments were conducted with an 8 μm track length at a constant velocity of 4 μm/s. All sliding experiments were repeated at least two times, and for some conditions, the sliding tests were repeated up to four times. The normal loads used for the experiments were varied between 0.2 and 5.0 mN, which resulted in a contact pressure between 0.4 and 3.5 GPa and a contact radius between 0.2 and 1.1 μm for the different tips. The total number of sliding cycles was 800, but due to limitation by the instrument software, only 400 cycles were performed at a time, and were repeated on the same position in order to achieve a total of 800 cycles. Each sliding test consisted of three phases, (1) a pre-scan, to image the topography at a 20 μN load, (2) an oscillating scratch, where the sample is worn under a constant load higher than 20 μN for 800 sliding cycles, and (3) a post-scan with 20 μN load to image the topography of the resulting wear trace. The

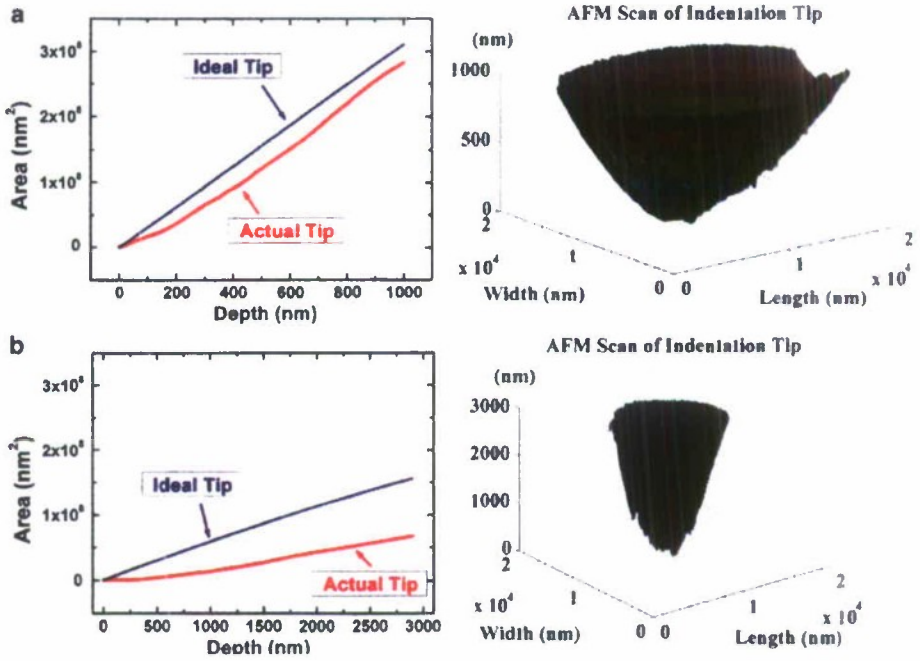

Fig. 1 Tip area function vs. depth obtained using an AFM scan for (a) the 50 μm tip and (b) the 10 μm tip

experimental method is described in more detail elsewhere [32].

The results from the sliding experiments were analyzed using a custom-built analysis code written with Matlab software. The coefficient of friction was calculated from the lateral force divided by the normal force. The average friction coefficient for each cycle was calculated from 75 (±2) data points corresponding to the central 5 μm of the track. For ex situ examination of wear, the wear track was scanned using an AFM operated in contact mode, and the wear volume was calculated from the cross-sectional area in the middle of the track multiplied by the length of the wear track.

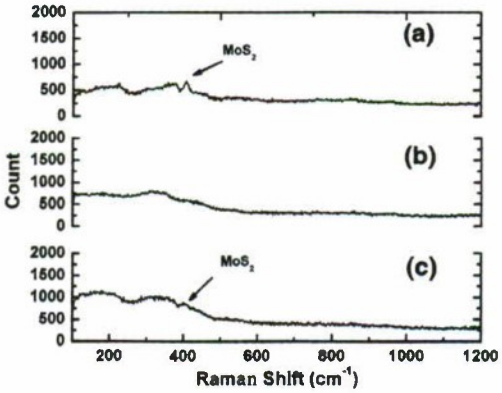

Fig. 2 Film characterization on the unworn surface using a Raman microscope for the (**a**) MoS_2, (**b**) Au–MoS_2, and (**c**) Ti–MoS_2 coating. Micro Raman scans show bands which are consistent with crystalline MoS_2 for the pure MoS_2 sample, however, no MoS_2 peaks are observed with the metal content samples

3 Results

3.1 Coating Characterization and Properties

Table 1 shows the properties of the coatings that were tested for this study. The hardness and the reduced modulus increased with the addition of metal to MoS_2. Also, the Ti–MoS_2 coating revealed higher reduced modulus and hardness values when compared to the Au-containing coating.

Figures 2a, b, and c shows Raman spectra for the MoS_2, Au–MoS_2, and Ti–MoS_2 samples, respectively. For the MoS_2 coating, the scan revealed peaks which are consistent with the Raman active modes for MoS_2(2H) [38–40]. A small peak at 408 cm^{-1} was also observed with the Ti–MoS_2 sample, however, no distinct MoS_2 peaks were observed with the Au content samples for the as-prepared coating. The broad features between 250 and 500 cm^{-1} are commonly seen in MoS_2 coatings that have a low degree of crystallinity. Results from X-ray diffraction measurements (not shown) revealed no peaks for crystalline phases in any of the coatings. Based on these two techniques, the coatings appear to be primarily amorphous, consistent with previous publications on these materials [23, 28].

3.2 Coefficient of Friction

Figure 3a, b, and c shows the average coefficient of friction versus the cycle number using a 50 μm tip for the MoS_2, Au–MoS_2, and Ti–MoS_2 samples, respectively. While three normal loads are plotted for each coating, sliding tests using normal loads in between and above the ones plotted were also performed and were used for the analysis in the discussion section. For all samples, both the run-in and steady-state coefficients of friction decrease with increasing normal load, which is typically observed for MoS_2 coatings.

A different behavior in the coefficient of friction is observed with the 10 μm tip sliding against the MoS_2, Au–MoS_2, and Ti–MoS_2 samples (see Fig. 4a, b, and c, respectively). The coefficient of friction does not decrease as significantly with increasing the normal load. In fact, the Au–MoS_2 sample reveals a higher friction coefficient with the highest normal load (see Fig. 4b). Furthermore, the MoS_2 sample shows an increase in the coefficient of friction with increasing the cycle number at the highest normal load (see Fig. 4a). Only the Ti–MoS_2 coating shows a similar, but not as significant, trend with the 10 μm tip (see Fig. 4c) when compared to the 50 μm tip (see Fig. 3c).

Overall, higher coefficients of friction are observed with the MoS_2 coating compared to the coatings with Au or Ti. Figure 5a and b shows the difference in coefficient of friction between the metal containing coatings and the pure MoS_2 coating, calculated from averaging the last 100 cycles. The difference in coefficient of friction between the MoS_2 sample and the metal containing samples decreases with increasing the normal load for the 50 μm tip. However, with increasing normal load for the 10 μm tip, the differences in coefficients of friction remain relatively similar. In some instances, the comparisons made in Fig. 5 are not representative of steady-state friction. That is, the friction coefficient for the MoS_2 sample never reaches steady state with the lowest normal load for the 50 μm tip, as it continuously increases throughout the whole test (see Fig. 3a).

Table 1 Coating properties of co-sputtered MoS_2, Au–MoS_2, and Ti–MoS_2

Sample	E_r (GPa)	H (GPa)	Thickness (nm)	RMS roughness (nm)
MoS_2	29 (±5)	1.2 (±0.4)	770	4.9
Au–MoS_2	68 (±8)	3.3 (±0.7)	330	5.2
Ti–MoS_2	118 (±9)	5.4 (±0.3)	870	3.3

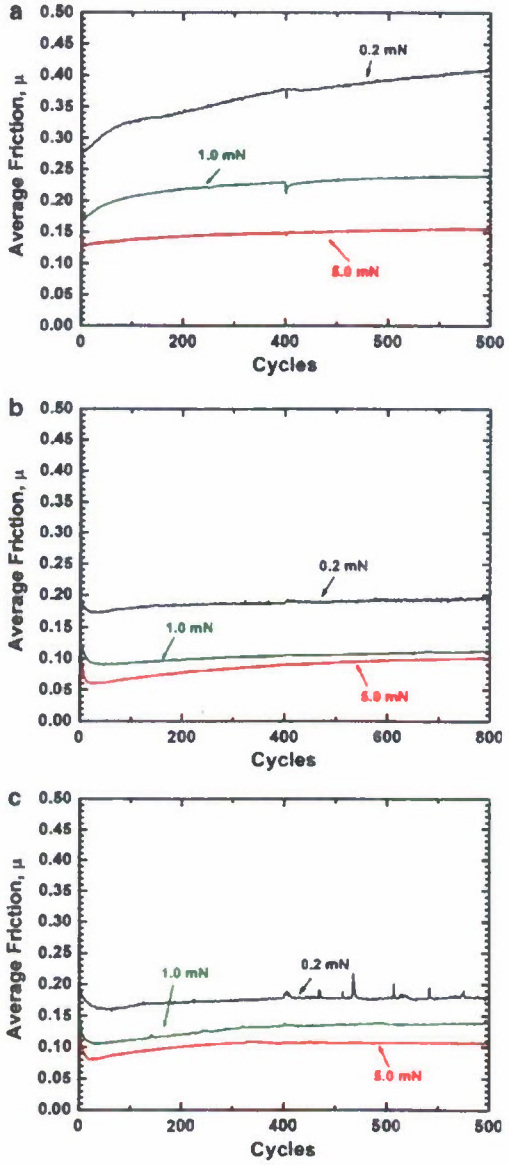

Fig.. 3 Average coefficient of friction vs. cycle number for the 50 μm using a normal load of 0.2mN, 1.0mN, and 5.0mN for (a) pure MoS_2, (b) Au–MoS_2, and (c) Ti–MoS_2 [Contact Stress: 0.4–1.2 GPa]

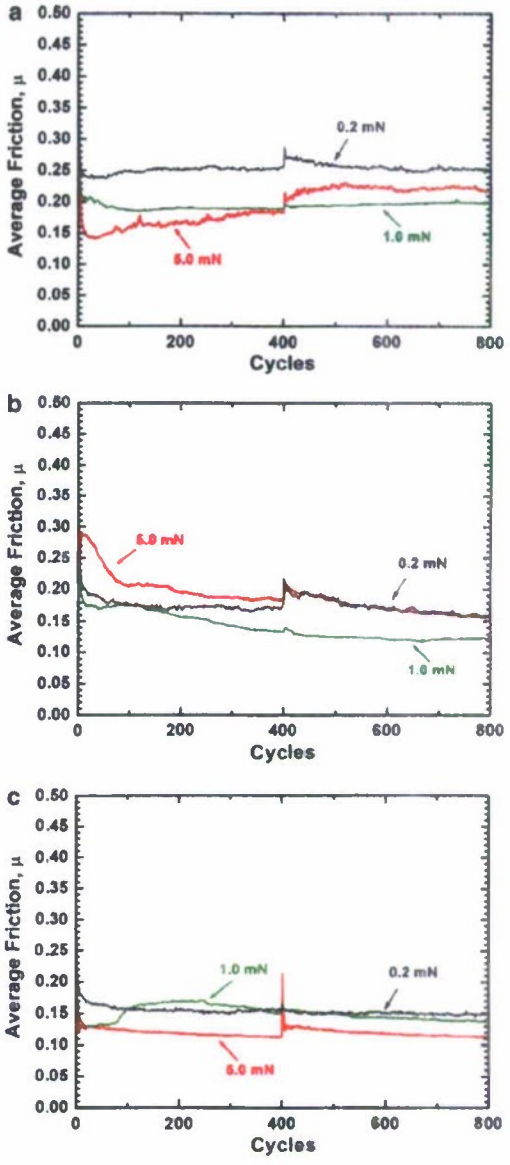

Fig. 4 Average coefficient of friction vs. cycle number for the 10 μm using a normal load of 0.2mN, 1.0mN, and 5.0mN for (a) pure MoS_2, (b) Au–MoS_2, and (c) Ti–MoS_2 [Contact Stress: 1.2–3.5GPa]

3.3 Wear Results

Figure 6a, b, and c shows cross-sectional profiles of the wear tracks on the MoS_2, Au–MoS_2, and Ti–MoS_2 coatings, respectively. Results are provided for both tips, each at three different loads. In most cases, there is a clear trend of increasing wear depth and volume with increasing load. However, for the largest load with the 10 μm tip on the Au–MoS_2 coating, there are flat regions within the wear track that correspond to the Si substrate. Wear data for these instances of coating failure were not used for further analysis. Figure 7a and b shows the wear volume for the 50 and 10 μm tip, respectively. The wear volume was plotted against the normal load, which varies between 0.2 and 5.0 mN. This corresponds to an initial Hertzian contact pressure between 0.4 and 1.2 GPa for the 50 μm tip and between 1.2 and 3.5 GPa for the 10 μm tip. For normal loads up to 1.0 mN with the 50 μm tip, very little wear is observed with the metal containing samples. In comparison to the MoS_2 coating, a magnitude in the wear volume similar to that for the coatings with Au and Ti was observed at the lowest loads (i.e. 0.2 and 0.5 mN).

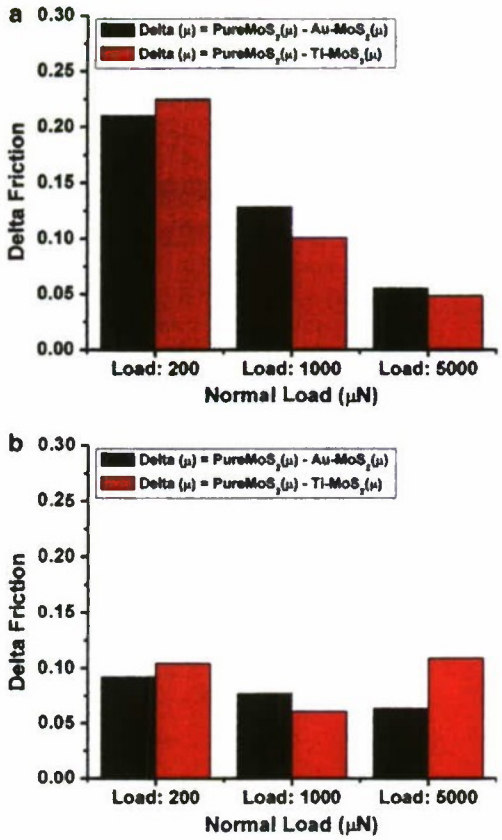

Fig. 5 "Delta friction," comparing the friction coefficients for the metal containing to the pure MoS_2 coatings for (a) the 50 μm Tip and (b) the 10 μm Tip

However, with the higher normal loads/contact pressures, the wear volume for the MoS_2 sample shows a linear increase when using the 50 μm tip, as seen in Fig. 7a.

The 10-μm tip shows a different behavior in the wear volume, as shown in Fig. 7b. For all samples, an increase in the wear volume is observed with increasing the normal load/contact pressure. Furthermore, with the highest contact pressure, the MoS_2 sample reveals the highest wear. It should be noted that for the highest contact pressure, the wear depth on the MoS_2 coating is higher than the actual coating thickness, indicating that the tip is sliding on the substrate. However, in Fig. 6a, one can see that the substrate is not exposed in the same way as for the thinner Au–MoS_2 coating for the same sliding conditions.

3.4 Surface Characterization and Adhesion Measurements

Figure 8 shows the pull-off force measured for the three different coatings. The highest pull-off force was seen with the pure MoS_2 coating followed by the Au–MoS_2 sample. The smallest pull-off force was seen with the Ti–MoS_2 sample.

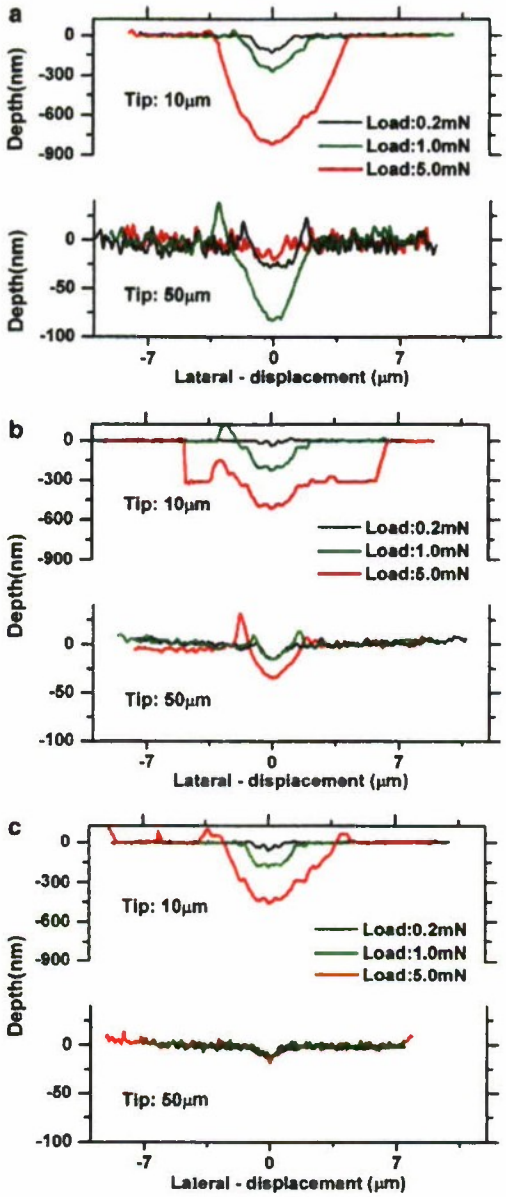

Fig. 6 Cross-sectional plots of the wear tracks, which were created using normal loads of 0.2, 1.0, and 3.0 mN and a tip radius of 10 and 50 μm on (a) Pure MoS_2, (b) Au–MoS_2, and (c) Ti–MoS_2 coatings

Figure 9a shows the film characterization of the worn surface using a Raman microscope for 10 μm tip using a normal load of 1.0 mN. For all the three coatings, the MoS_2 peaks observed for the worn surface are more distinct than prior to sliding (c.f. Fig. 2). Similar results were obtained for the 10 μm tip using a normal load of 0.2 mN (see Fig. 9b). However, the peaks for the Au–MoS_2 coating remained rather indistinct for this sliding condition. For sliding with the 50 μm tip on the Au–MoS_2 sample and

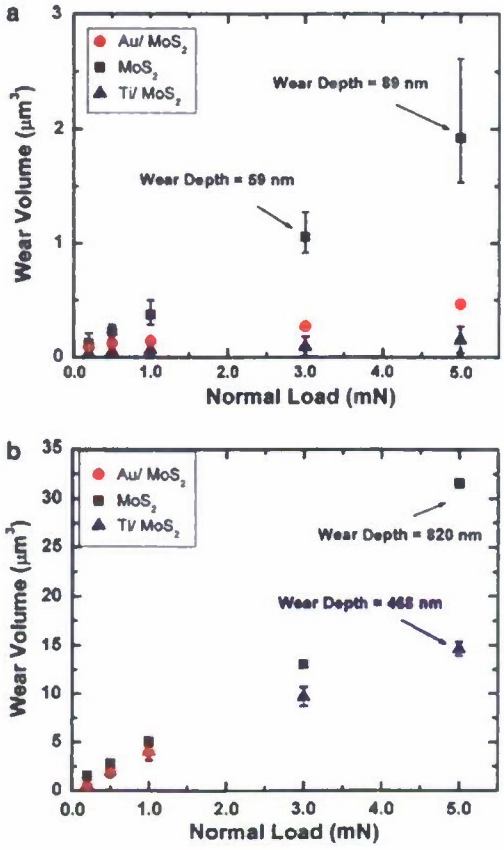

Fig. 7 Wear volume vs. normal load for the (a) 50 m tip and (b) 10 m tip

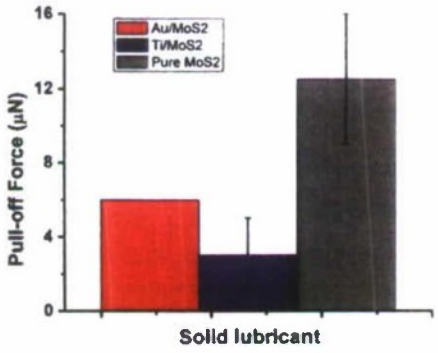

Fig. 8 Pull-off force measurements on the three different coatings

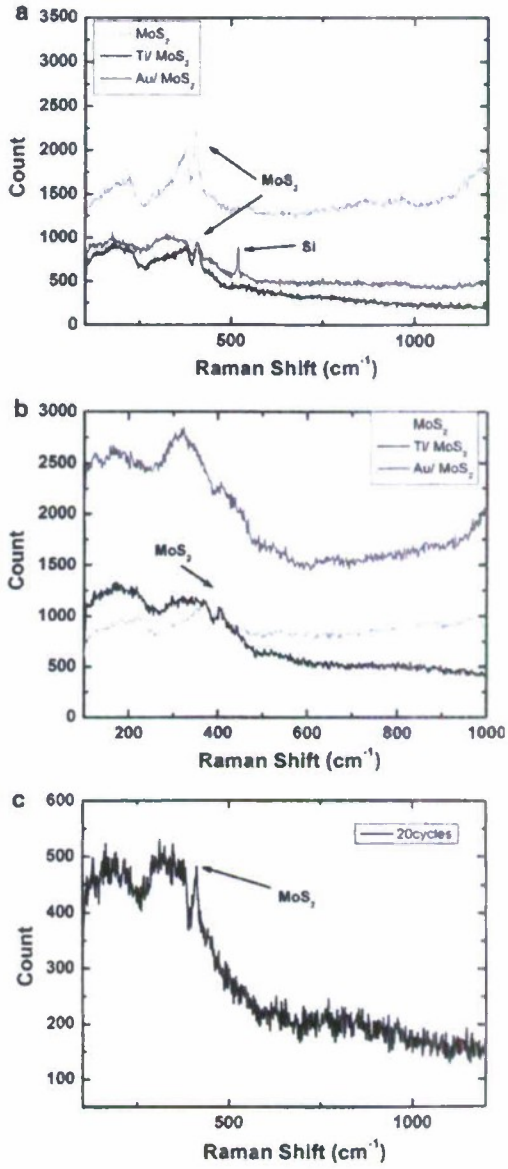

Fig. 9 Film characterization of the worn surface using a Raman microscope for the (a) 10 μm tip using a normal load of 1.0 mN, (b) 10 μm tip using a normal load of 0.2 mN, and (c) 50 μm tip on the Au–MoS_2 coating using a normal load of 5.0 mN after 20 cycles. Micro Raman scans show bands which are consistent with crystalline MoS_2 for all samples. Crystalline MoS_2 is also seen by as few as 20 cycles

using a normal load of 5.0 mN, evidence of MoS_2 tribofilm formation was seen in as few as 20 cycles (see Fig. 9c).

4 Discussion

In comparing the performance of Ti–MoS_2 and Au–MoS_2 coatings to the pure MoS_2 coatings, it is first relevant to compare to macrotribology results in the literature [25–27, 29]. In general, metal is added to MoS_2 to enhance the mechanical and tribological properties, especially in the regime of higher relative humidity. Simmonds et al. studied the tribology of both Au–MoS_2 [29] and Ti–MoS_2 [25] coatings in 50% RH with an initial contact stress of 1 GPa. For Au–MoS_2 coatings with a similar Au content to those studied here, they observed a reduction of the friction

coefficient from 0.17 to 0.15 as compared to pure MoS_2 and an increase in the endurance. For Ti–MoS_2 coatings with a similar Ti content to those studied here, they observed a reduction of the friction coefficient from 0.18 to 0.07 as compared to pure MoS_2. Zabinski et al. [26] studied Au–MoS_2 coatings with pin-on-disk tribometry with an initial contact stress of 0.98 GPa and found a reduction in the friction coefficient compared to pure MoS_2 in both dry (3–5% RH) and ambient conditions. For the coatings studied here, previous macrotribology research on Au–MoS_2 [23] and Ti–MoS_2 [24, 28] demonstrated friction reduction and increase in endurance compared to pure MoS_2. The magnitude of the friction reduction in microtribology (c.f. Fig. 5) was found to be similar to the macrotribology results. For a load of 5.0 mN on the 50 μm tip and 0.2 mN on the 10 μm tip, the initial contact stress is 1.2 GPa, similar to the stress in the macroscopic studies. The reduction in friction coefficient observed here is between 0.05 and 0.1. Despite the significant differences in %RH, this result compares favorably to those of Simmonds et al. [25, 29], who saw a reduction in friction of 0.02 for Au–MoS_2 and 0.11 for Ti–MoS_2. Zabinski et al. [26] observed a reduction in friction of 0.03 in dry conditions for Au–MoS_2 compared to pure MoS_2. Thus, a similar friction-reducing capability of metal doping of MoS_2 is also observed for microtribology. Without running longer tests, it is not clear whether the same can be said for the effect on coating endurance. However, the wear for the Ti–MoS_2 and Au–MoS_2 coating were consistently less when compared to pure MoS_2 (c.f. Fig. 7), especially at higher contact stresses.

Other observations of the microtribology experiments on MoS_2 and metal-doped MoS_2 coatings showed both additional similarities and some subtle differences to macrotribology. The steady-state friction force (i.e. 800th cycle) was plotted against the normal force in log–log plots, Fig. 10a and b for the 50 and 10 μm tip, respectively. A linear fit was conducted on the results according to $F \propto L^m$, where m is the slope of the fit in the log–log scale. The linear fit showed that the m value was 0.94, 0.89, and 0.94 when using the 10 μm tip and 0.78, 0.79, and 0.84 when using the 50 μm tip for the MoS_2, Au–MoS_2, and Ti–MoS_2, coatings, respectively. This indicates that with the 10 μm tip, all three coatings show higher m values when compared to the 50 μm tip. Furthermore, when using the 50 μm tip, the MoS_2 coating follows the relationship of $F \propto L^{0.78}$, which is closer to $F \propto L^{2/3}$ when compared to the other two coatings and the 10 μm tip. The Hertzian behavior of $F \propto L^{2/3}$ has been previously observed in macrotribology studies of MoS_2 coatings by Singer et al. [41, 42] and by several other authors [30, 43]. The higher m values with the 10 μm tip can be explained by the difference in the tip shape, as seen in Fig. 1b. The difference

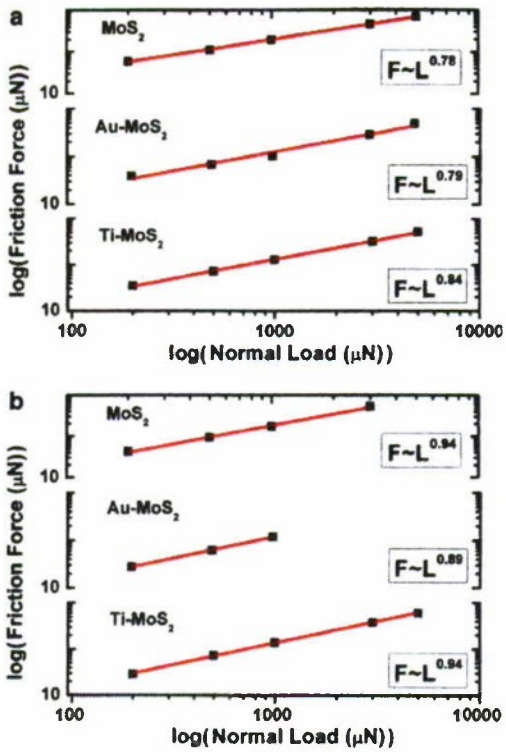

Fig. 10 Friction force vs. Normal load for (**a**) the 50-μm tip a nd (**b**) the 10-μm tip for sputtered MoS_2 sample and co-sputtered Au–MoS_2 sample and co-sputtered Ti–MoS_2 sample

between the actual area function (i.e. measured using an AFM) and the ideal area function (i.e. ideal shape of a sphere) of the 10-μm tip is greater than the 50-μm tip. The 10-μm tip deviates from a spherical shape, which can cause a different F to L relationship. It has previously been shown that even small deviations from a spherical tip shape can result in increasing m values as high as one [44], as seen in our case with the 10 μm tip.

As described in the literature [41, 43, 45, 46], the shear strength has a pressure dependence which can be approximated by

$$S = S_o + \alpha P \tag{1}$$

where S_o is the interfacial shear strength also called the "velocity accommodation parameter," P is the mean pressure of the contact, and α represents the limiting coefficient of friction [41]. This equation is often cast in terms of the coefficient of friction, μ, such that

$$\mu = S_o/P + \alpha \tag{2}$$

Thus, from Eq. 2, the coefficient of friction is inversely proportional to the pressure. This behavior was also confirmed when plotting the steady-state friction coefficient (800th cycle) versus inverse pressure for the 50-μm tip on the MoS_2, Au–MoS_2, and Ti–MoS_2 coatings (see

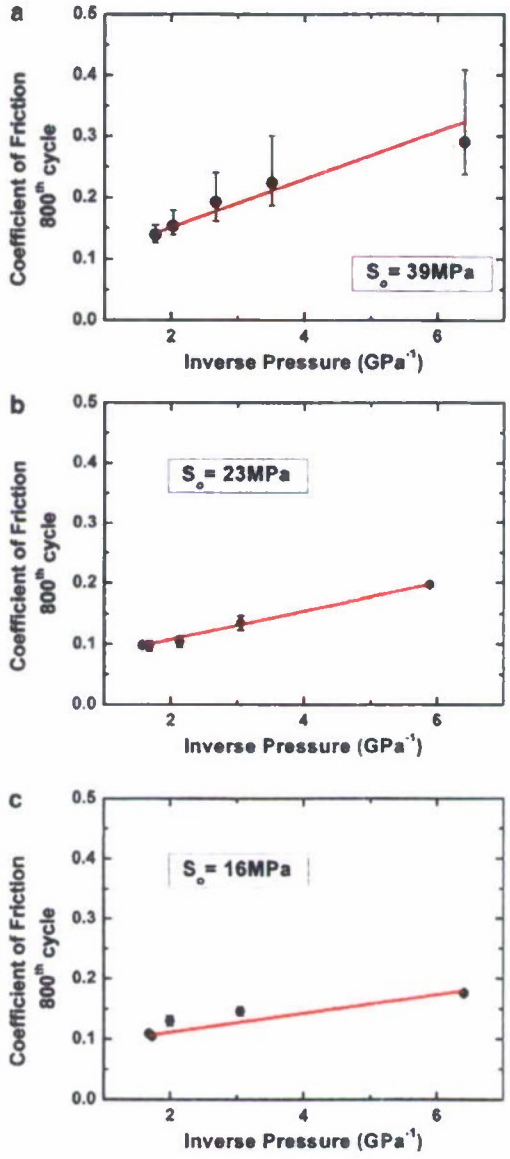

Fig. 11 Coefficient of friction vs. inverse pressure using the 50 μm for (**a**) sputtered MoS_2 sample and (**b**) co-sputtered Au–MoS_2 sample and (**c**) co-sputtered Ti–MoS_2 sample. Linear fit was performed on each coating and the slope (S_o) and intercept (α) were obtained following the equation of $\mu = S_o/P + \alpha$. The contact pressure is calculated at the 800th cycle using the actual area function of the tip

Figs 11a, b, and c, respectively). The pressure for this plot was calculated at the steady-state condition (800th cycle) using the normal force divided by the projected area of the tip. The area was determined from the results of the pixel-counting algorithm of AFM images (see Fig. 1). The value of the tip area at the 800th cycle was calculated using the elastic depth, which was obtained from the difference in the normal displacement of the post-scan (i.e. 3rd phase of the sliding experiment) and the last sliding cycle.

Least square fit of a straight line was performed on each sample for the 50 μm tip, shown in Fig. 11a, b, and c. Reasonable fits were not obtained for the 10 μm tip (not shown). This may be explained by the fact that not enough data points were used, because the tip was often in contact with the substrate at the higher normal loads. Furthermore, the higher contact pressures obtained with the 10 μm tip could also result in higher plowing, which leads to difficulty in measuring the actual contact area.

The fit with the 50-μm tip revealed a mean slope (S_o) and an intercept (α) for each sample, and the values are summarized in Table 2. The velocity accommodation parameter, S_o, decreases with the addition of metal to MoS_2. Also, the mean slope S_o shows the lowest value (15 MPa) with the Ti content sample when compared to the other two samples (39 and 23 MPa for the MoS_2 and the Au–MoS_2 samples, respectively). The y-intercept, α, showed similar values for all three coatings (see Table 2). The lower S_o values for the Ti and Au coating compare favorably with S_o values obtained in macrotribology, for MoS_2 coatings, at low relative humidity levels [42] where low friction values were observed. The value for the pure MoS_2 coating is slightly higher than typically observed [41]. Considering that the higher wear at the larger normal loads for the MoS_2 coating may be affecting this analysis, a fit was conducted to the three data points for the lower normal loads. This results in a shear strength of 26 MPa, but with much higher uncertainty due to the large scatter in friction data for the lowest loads on the MoS_2 coating. Thus, we believe that the pure MoS_2 did give a similar response at the lower loads to the other coating and similar shear strength to the literature on macroscopic contacts on MoS_2.

Table 2 Microtribological properties summary for testing with the 50 μm tip

	Wear volume (μm^3) [L: 3.0/5.0mN]	S_o (MPa)	α	Friction (μ) [L: 3.0/5.0 mN]	Friction force
MoS_2	1.1/1.9	39 (±6)	0.07(±0.01)	0.15/0.14	$F \propto L^{0.78}$
Au–MoS_2	0.3/0.5	23.2 (±0.4)	0.061(±0.002)	0.10/0.10	$F \propto L^{0.79}$
Ti–MoS_2	0.1/0.2	15 (±3)	0.079(±0.006)	0.11/0.10	$F \propto L^{0.84}$

Further examination of data in Table 2 allows for comparisons of the hardness, velocity accommodation parameter (S_o), wear volume, coefficient of friction, and friction force relationship with normal load. In terms of the relationship between the friction force and the normal force (i.e. $F \propto L^m$) the pure MoS_2 sample shows the closest value to 2/3, when compared to the two other coatings. However, the m value for the metal doped samples is very similar to the m value of the pure MoS_2 sample. Also, the limiting friction is similar for all coatings, and S_o is, in all cases, low and relatively comparable to measurements at macroscopic length scales [30, 41–43]. However, the hardness was observed to increase with the addition of metal to MoS_2, and the highest hardness value was obtained with the Ti content sample followed by the Au–MoS_2 coating. This can be directly correlated with the wear volume of the three different coatings. The wear volume decreases with the addition of metal to MoS_2 and therefore decreases with increasing the hardness. As seen with the hardness values, the highest wear resistance is also observed with the Ti content sample.

While the wear resistance of a coating can sometimes simply be explained by the hardness, further analysis of the wear mechanisms was carried out using a modified version of the technique of Kuster and Schiffmann [16]. In their method, the wear contribution is separated into two components and directly correlated to the total depth during a sliding process, which consists of three contributions: elastic deformation, plastic deformation, and removed material. Kuster and Schiffmann [16] used three depth values in order to calculate each wear contribution; the depth after the initial loading (D_{IL}), the depth under normal load after the last cycle of the test (D_{LC}), and the residual depth after unloading measured from the end scan (D_{RD}). Using these measurements, the following equations can be derived:

$$\text{Elastic deformation} = D_{LC} - D_{RD}, \tag{3}$$

$$\text{Removed material} = D_{LC} - D_{IL}, \tag{4}$$

$$\begin{aligned}\text{Plastic deformation} &= D_{RD} - [\text{Removed material}] \\ &= D_{RD} - (D_{LC} - D_{IL}).\end{aligned} \tag{5}$$

We used a slightly modified version of this method because it was difficult to measure the wear depth from the end scan of the sliding test (due to thermal drift and material pile up at the end of the wear track). Thus, the value of D_{IL} was calculated using the elastic–plastic wear depth from an indentation test and the value of D_{RD} was calculated using the wear depth obtained with an AFM.

The different depth contributions versus the normal loads for the 50-μm tip are plotted in Fig. 12a, b, and c for the pure MoS_2, Au–MoS_2, and Ti–MoS_2 coatings, respectively. The highest plastic deformation is observed with the pure MoS_2 coating, which can be explained by the lower

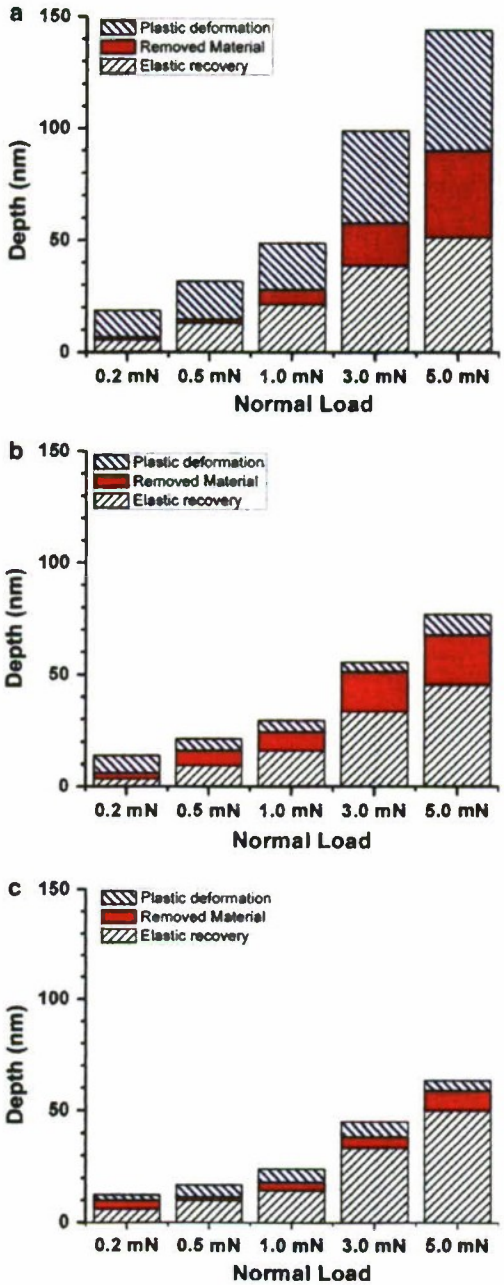

Fig. 12 Depth contribution during a sliding test using the 50 μm tip for (a) pure MoS_2, (b) Au–MoS_2, and (c) Ti–MoS_2

hardness value. The Au and Ti content samples show similar contribution of plastic deformation to the wear, which is a smaller when compared to the one of the pure MoS_2 samples. However, the removed material is slightly higher with the Au content sample when compared to the Ti content sample and the highest contribution of removed material to the total depth is seen with the pure MoS_2 sample. For those loads that could be analyzed for the

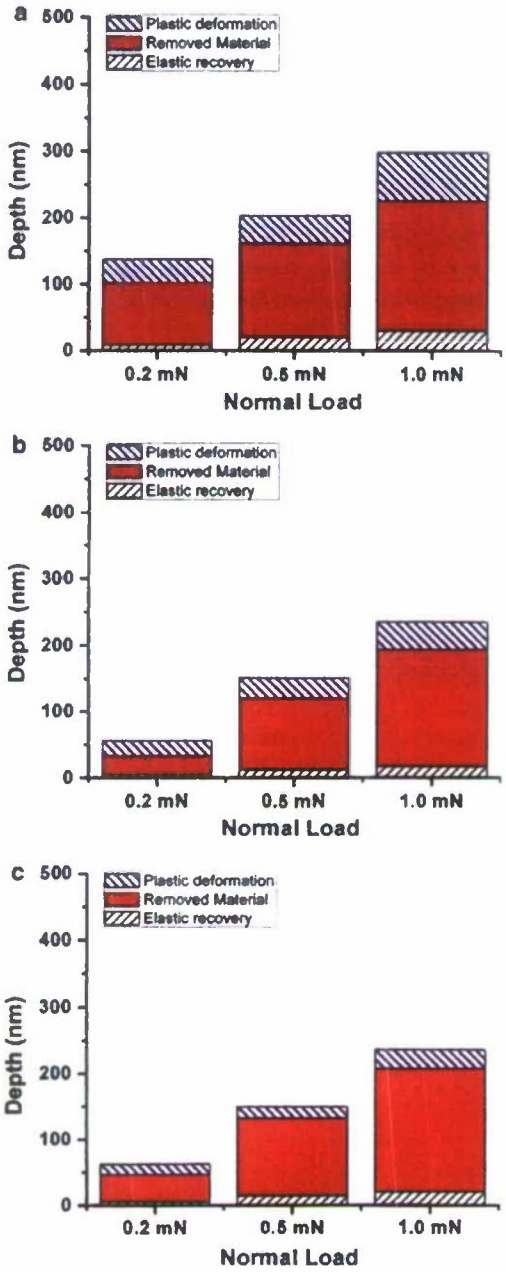

Fig. 13 Depth contribution during a sliding test using the 10 μm tip for (**a**) pure MoS_2, (**b**) Au–MoS_2, and (**c**) Ti–MoS_2

10 μm tip, similar results were observed (see Fig. 13a, b, and c for the pure MoS_2, Au–MoS_2, and Ti–MoS_2 coatings, respectively).

The removed material can be correlated to either plowed material or adhesive wear. While some plowing must occur during our tests, our steady-state analysis for the 50-μm tip revealed a nearly Hertzian relationship between the friction and the normal load. The small deviation from $L^{2/3}$, while possibly attributable to tip shape, may also be due to adhesion. Thus, differences in removed material might be also due to differences in the surface adhesion. As seen in Fig. 8, the highest pull-off force was seen with the pure MoS_2 coating followed by the Au–MoS_2 sample and the smallest pull-off force was seen with the Ti–MoS_2 sample. Thus, if adhesive wear is part of the removed material, these measurements help to explain the trend in wear resistance of the coatings. The adhesion measurements are also consistent with the velocity accommodation parameter, S_o, which shows the same trend with decreasing interfacial shear strength from MoS_2 to Au–MoS_2 to Ti–MoS_2. It has been previously suggested that the S_o value represents a property of the interfacial shear strength between the transfer film (i.e. MoS_2 transferred on the tip) and the tribofilm [41] (i.e. crystalline MoS_2 on the surface of the wear track), but could also include the shear strength of each film, depending on which velocity accommodation mode is active. The decrease in surface adhesion with the decrease in the S_o value may indicate that the metal-doped samples form a uniform and stable transfer- and tribo-film, leading to lower interfilm shear strength.

It has been previously shown with macro- and nano-tribology [8, 21], that a crystalline tribofilm is formed on the worn surface of the MoS_2 film, which contributes to a low shear stress and therefore a low coefficient of friction. This typically occurs in the run-in stage, where the basal planes become oriented in a parallel direction to the sliding path and transfer occurs to the counterface. Similar behavior on the wear track may also be expected with microtribology. While the spectra presented in Fig. 9 provide significant evidence of tribofilm formation on the wear track, additional experiments with Raman spectroscopy on the counterfaces revealed no peaks for MoS_2. Of course, a transfer film could be present that is either in such small quantity or such an amorphous state as to be undetectable by Raman spectroscopy. It should also be mentioned that while the evidence in Fig. 9 was the predominant observation from the Raman studies, other tests revealed no peaks that would indicate tribofilm formation. Additional surface characterization experiments will be necessary to unambiguously determine the role of transfer films in microtribology on solid lubricant coatings such as those studied here.

5 Conclusion

The microtribological properties of co-sputtered Ti and Au with MoS_2 solid lubricants were investigated, with a wide range of contact pressures. It was observed that the small addition of Ti and Au to MoS_2 improved the tribological properties in dry air; the co-sputtered Ti and Au with MoS_2 solid lubricants showed lower friction and less wear

compared to the pure MoS_2 coating. The improved tribological properties with metal additions were attributed to an increase in the mechanical properties, decrease in adhesion, and a decrease in the interfacial shear strength or 'velocity accommodation parameter'. The interfacial shear strength for the Ti and Au content samples was similar to literature values obtained at the macroscale, indicating a similar sliding behavior. This was also confirmed with the evidence of a tribofilm on the surface of the wear tracks, which was seen with Raman spectroscopy.

Acknowledgments The authors gratefully acknowledge financial support from Fonds québécois de la recherche sur la nature et les technologies (FQRNT), program Établisssement de nouveaux chercheurs and Lorne Trottier for the graduate Fellowship (McGill Engineering Doctoral Award). This study was also supported under The Aerospace Corporation's Mission Oriented Investigation and Experimentation program, funded by the U.S. Air Force Space and Missile Systems Center under Contract No. FA8802-09-C-0001. The authors acknowledge Zachary Fishman for his collaboration with the Matlab code. The assistance of Francois Barthelet in conducting atomic force microscopy measurements is also gratefully acknowledged.

References

1. Bhushan, B.: In: Bhushan, B. (ed.) Handbook of Micro/Nano Tribology, pp. 797–834. CRC Press, Boca Raton, FL (1999)
2. Bora, C.K., Flater, E.E., Street, M.D., Redmond, J.M., Starr, M.J., Carpick, R.W., Plesha, M.E.: Multiscale roughness and modeling of MEMS interfaces. Tribol. Lett. (USA) **19**(1), 37–48 (2005)
3. Delrio, F.W., De Boer, M.P., Knapp, J.A., Reedy Jr, E. D., Clews, P.J., Dunn, M.L.: The role of van der Waals forces in adhesion of micromachined surfaces. Nat. Mater. **4**(8), 629–634 (2005)
4. Dugger, M.T.: Surface treatments for modifying the tribological behavior of microsystems. In: Proceedings of the World Tribology Congress III - 2005, pp. 711–713. American Society of Mechanical Engineers, New York, NY (2005)
5. Gee, M.G., Gee, A.D.: A cost effective test system for microtribology experiments. Wear (Netherlands) **263**(7–12 SPEC. ISS), 1484–1491 (2007)
6. Liu, H.W., Bhushan, B.: Adhesion and friction studies of microelectromechanical systems/nanoelectromechanical systems materials using a novel microtriboapparatus. J. Vac. Sci. Technol. A **21**(4), 1528–1538 (2003)
7. Nosonovsky, M., Bhushan, B.: Scale effect in dry friction during multiple-asperity contact. Trans. ASME, J. Tribol. (USA) **127**(1), 37–46 (2005)
8. Kim, H., Lince, J.R.: Direct visualization of sliding-induced tribofilm on Au/MoS_2 nanocomposite coatings by c-AFM. Tribol. Lett. **26**(1), 61–65 (2007)
9. Schiffmann, K.I.: Microtribological/mechanical testing in 0, 1 and 2 dimensions: a comparative study on different materials. Wear (Netherlands) **265**(11–12), 1826–1836 (2008)
10. Lince, J.R., Kim, H.I., Adams, P.M., Dickrell, D.J., Dugger, M.T.: Nanostructural, electrical, and tribological properties of composite Au–MoS_2 coatings. Thin Solid Films **517**(18), 5516–5522 (2009)
11. Deladi, S., Berenschot, J. W., De Boer, M. J., Krijnen, G. J. M., Elwenspoek, M. C.: In: Proceedings of the 17th IEEE International Conference on Micro Electro Mechanical Systems (MEMS), pp. 181–184. Institute of Electrical and Electronics Engineers Inc., Maastricht, Netherlands (2004)
12. Schiffmann, K.I., Hieke, A.: Analysis of microwear experiments on thin DLC coatings: friction, wear and plastic deformation. Wear (Netherlands) **254**(5–6), 565–572 (2003)
13. Ahmed, S.I.U., Bregliozzi, G., Haefke, H.: Microfrictional properties of diamond-like carbon films sliding against silicon, sapphire and steel. Wear (Netherlands) **254**(11), 1076–1083 (2003)
14. Bandorf, R., Luthje, H., Staedler, T.: Influencing factors on microtribology of DLC films for MEMS and microactuators. Diam. Relat. Mater. (Netherlands) **13**(4–8), 1491–1493 (2004)
15. Chromik, R.R., Wahl, K.J.: Friction of microscale contacts on diamond-like carbon nanocomposite coatings. In: Proceedings of the World Tribology Congress III - 2005, pp. 829–830. American Society of Mechanical Engineers, New York, NY (2005)
16. Kuster, R.L.A., Schiffmann, K.I.: Nano-scratch testing on thin diamond-like carbon coatings for microactuators: friction, wear and elastic-plastic deformation. Z. Met.kd. (Germany) **95**(5), 306–310 (2004)
17. Bhushan, B.: Chemical, mechanical and tribological characterization of ultra-thin and hard amorphous carbon coatings as thin as 3.5 nm: recent developments. Diam. Relat. Mater. (Netherlands) **8**(11), 1985–2015 (1999)
18. Bhushan, B., Liu, H.W., Hsu, S.M.: Adhesion and friction studies of silicon and hydrophobic and low friction films and investigation of scale effects. J. Tribol. Trans. ASME **126**(3), 583–590 (2004)
19. Scharf, T.W., Prasad, S.V., Dugger, M.T., Kotula, P.G., Goeke, R.S., Grubbs, R.K.: Growth, structure, and tribological behavior of atomic layer-deposited tungsten disulphide solid lubricant coatings with applications to MEMS. Acta Mater. (UK) **54**(18), 4731–4743 (2006)
20. Scharf, T.W., Prasad, S.V., Dugger, M.T., Mayer, T.M.: Atomic layer deposition of solid lubricant thin films. In: Proceedings of the World Tribology Congress III - 2005, pp. 375–376. American Society of Mechanical Engineers, New York, NY (2005)
21. Dvorak, S.D., Wahl, K.J., Singer, I.L.: In situ analysis of third body contributions to sliding friction of a Pb–Mo–S coating in dry and humid air. Tribol. Lett. **28**(3), 263–274 (2007)
22. Wahl, K.J., Seitzman, L.E., Bolster, R.N., Singer, I.L.: Low-friction, high-endurance, ion-beam-deposited Pb–Mo–S coatings. Surf. Coat. Technol. **73**(3), 152–159 (1995)
23. Lince, J.R.: Tribology of co-sputtered nanocomposite Au/MoS_2 solid lubricant films over a wide contact stress range. Tribol. Lett. (USA) **17**(3), 419–428 (2004)
24. Renevier, N.M., Fox, V.C., Teer, D.G., Hampshire, J.: Performance of low friction MoS2/titanium composite coatings used in forming applications. Mater. Des. **21**(4), 337–343 (2000)
25. Simmonds, M.C., Savan, A., Pfluger, E., Van Swygenhoven, H.: Mechanical and tribological performance of MoS2 co-sputtered composites. Surf. Coat. Technol. (Switzerland) **126**(1), 15–24 (2000)
26. Zabinski, J.S., Donley, M.S., Walck, S.D., Schneider, T.R., McDevitt, N.T.: Effects of dopants on the chemistry and tribology of sputter-deposited MoS_2 films. Tribol. Trans. **38**(4), 894–904 (1995)
27. Spalvins, T.: Frictional and morphological properties of Au–MoS_2 films sputtered from a compact target. Thin Solid Films **118**(3), 375–384 (1984)
28. Wang, X., Xing, Y., Ma, S., Zhang, X., Xu, K., Teer, D.G.: Microstructure and mechanical properties of MoS_2/titanium composite coatings with different titanium content. Surf. Coat. Technol. **201**(9–11 SPEC. ISS), 5290–5293 (2007)
29. Simmonds, M.C., Savan, A., Pflüger, E., Van Swygenhoven, H.: Microstructure and tribological performance of MoSx/Au co-sputtered composites. J. Vac. Sci. Technol. Part A Vac. Surf. Films **19**(2), 609–613 (2001)

30. Grosseau-Poussard, J.L., Moine, P., Brendle, M.: Shear strength measurements of parallel MoS_x thin films. Thin Solid Films (Switzerland) **307**(1–2), 163–168 (1997)
31. Lansdown, A.R.: Molybdenum disulphide lubrication. Elsevier Science B.V, Amsterdam (1999)
32. Stoyanov, P., Fishman, J.Z., Lince, J.R., Chromik, R.R.: Microtribological performance of MoS_2 lubricants with varying Au content. Surf. Coat. Technol. (Switzerland) **203**(5–7), 761–765 (2008)
33. Stoyanov, P., Lince, J.R., Chromik, R. R.: Micro-scale sliding contacts on Au and Au–MoS_2 coatings. submitted to Surf. Coat. Technol. (2010)
34. Sahoo, R.R., Biswas, S.K.: Microtribology and friction-induced material transfer in layered MoS_2 nanoparticles sprayed on a steel surface. Tribol. Lett. **37**(2), 313–326 (2010)
35. Sahoo, R.R., Math, S., Biswas, S.K.: Mechanics of deformation under traction and friction of a micrometric monolithic MoS_2 particle in comparison with those of an agglomerate of nanometric MoS_2 particles. Tribol. Lett. **37**(2), 239–249 (2010)
36. Nair, R.P., Zou, M.: Surface-nano-texturing by aluminum-induced crystallization of amorphous silicon. Surf. Coat. Technol. **203**(5–7), 675–679 (2008)
37. Bushby, A.J., Jennett, N.M.: Determining the area function of spherical indenters for nanoindentation. In: Baker, S.P., Cook, R.F., Corcoran, S.G., Moody, N.R. (eds.) Fundamentals of Nanoindentation and Nanotribology II, vol. 649, pp. Q7.17.11–Q17.17.16. Materials Research Society, Warrendale, PA (2001)
38. Shin, H., Doer, H.J., Deshpandey, C., Fuqua, P., Dunn, B., Bunshah, R.F.: Effect of niobium doping on the properties of molybdenum sulfides as cathode materials. Surf. Coat. Technol. **36**(3–4), 859–865 (1988)
39. Wahl, K.J., Dunn, D.N., Singer, I.L.: Effects of ion implantation on microstructure, endurance and wear behavior of IBAD MoS_2. Wear (Netherlands) **237**(1), 1–11 (2000)
40. Wieting, T.J., Verble, J.L.: Infrared and Raman studies of long-wavelength optical phonons in hexagonal MoS_2. Phys. Rev. B **3**(12), 4286 (1971)
41. Singer, I.L.: Solid lubrication processes. In: Singer, I.L., Pollock, H.M. (eds.) Fundamentals of Friction, pp. 237–261. Kluwer Academic Publishers, Dordrecht (1992)
42. Singer, I.L., Bolster, R.N., Wegand, J., Fayeulle, S., Stupp, B.C.: Hertzian stress contribution to low friction behavior of thin MoS_2 coatings. Appl. Phys. Lett. **57**(10), 995–997 (1990)
43. Briscoe, B.J., Smith, A.C.: The interfacial shear strength of molybdenum disulfide and graphite films. Tribol. Trans. **25**(3), 349–354 (1982)
44. Schwarz, U.D., Zwörner, O., Köster, P., Wiesendanger, R.: Quantitative analysis of the frictional properties of solid materials at low loads. I. Carbon compounds. Phys. Rev. B **56**(11), 6987 (1997)
45. Bridgeman, P.W.: Shearing phenomena at high pressure particularly in inorganic compounds. In: Proceedings of the American Academy of Arts and Sciences, vol. 71, p. 387 (1936)
46. Erdemir, A., Erck, R.A., Robles, J.: Relationship of hertzian contact pressure to friction behavior of self-lubricating boric acid films. Surf. Coat. Technol. **49**(1–3), 435–438 (1991)

PHYSICAL SCIENCES LABORATORIES

The Aerospace Corporation functions as an "architect-engineer" for national security programs, specializing in advanced military space systems. The Corporation's Physical Sciences Laboratories support the effective and timely development and operation of national security systems through scientific research and the application of advanced technology. Vital to the success of the Corporation is the technical staff's wide-ranging expertise and its ability to stay abreast of new technological developments and program support issues associated with rapidly evolving space systems. Contributing capabilities are provided by these individual organizations:

Electronics and Photonics Laboratory: Microelectronics, VLSI reliability, failure analysis, solid-state device physics, compound semiconductors, radiation effects, infrared and CCD detector devices, data storage and display technologies; lasers and electro-optics, solid-state laser design, micro-optics, optical communications, and fiber-optic sensors; atomic frequency standards, applied laser spectroscopy, laser chemistry, atmospheric propagation and beam control, LIDAR/LADAR remote sensing; solar cell and array testing and evaluation, battery electrochemistry, battery testing and evaluation.

Space Materials Laboratory: Evaluation and characterizations of new materials and processing techniques: metals, alloys, ceramics, polymers, thin films, and composites; development of advanced deposition processes; nondestructive evaluation, component failure analysis and reliability; structural mechanics, fracture mechanics, and stress corrosion; analysis and evaluation of materials at cryogenic and elevated temperatures; launch vehicle fluid mechanics, heat transfer and flight dynamics; aerothermodynamics; chemical and electric propulsion; environmental chemistry; combustion processes; space environment effects on materials, hardening and vulnerability assessment; contamination, thermal and structural control; lubrication and surface phenomena. Microelectromechanical systems (MEMS) for space applications; laser micromachining; laser-surface physical and chemical interactions; micropropulsion; micro- and nanosatellite mission analysis; intelligent microinstruments for monitoring space and launch system environments.

Space Science Applications Laboratory: Magnetospheric, auroral and cosmic-ray physics, wave-particle interactions, magnetospheric plasma waves; atmospheric and ionospheric physics, density and composition of the upper atmosphere, remote sensing using atmospheric radiation; solar physics, infrared astronomy, infrared signature analysis; infrared surveillance, imaging and remote sensing; multispectral and hyperspectral sensor development; data analysis and algorithm development; applications of multispectral and hyperspectral imagery to defense, civil space, commercial, and environmental missions; effects of solar activity, magnetic storms and nuclear explosions on the Earth's atmosphere, ionosphere and magnetosphere; effects of electromagnetic and particulate radiations on space systems; space instrumentation, design, fabrication and test; environmental chemistry, trace detection; atmospheric chemical reactions, atmospheric optics, light scattering, state-specific chemical reactions, and radiative signatures of missile plumes.